Polycrystalline LPCVD 3C-SiC Thin Films on SiO_2 Using Alternating Supply Deposition

Philipp Moll, Georg Pfusterschmied, Sabine Schwarz, Werner Artner, and Ulrich Schmid

***Abstract*— In this paper, we demonstrate the deposition of 3C-SiC thin films on SiO_2 using the alternating supply deposition (ASD) technique in a low-pressure chemical vapor deposition (LPCVD) furnace. We provide data of the thin film properties showing strong dependencies on the process gas flow rates of silane, propane and hydrogen. For comparative reasons all gas flow compositions were performed on <100> silicon and SiO_2. A decreased rate of growth per cycle of ∼37 % was discovered on SiO_2. X-ray photoelectron spectroscopy (XPS) depth profiling revealed an oxygen content of 7.5 % ±2.5 % throughout the entire thin film when grown on SiO_2. High resolution transmission electron microscopy (HRTEM) showed a 15 nm amorphous carbon layer at the 3C-SiC/Si interface. Conversely, on SiO_2 a 10 nm graphite layer was determined as intermediate layer leading to prominent <111> 3C-SiC X-ray diffraction (XRD) peaks. Independent of the substrate type a similar microstructure is observed in cross-sectional analyses. Atomic force microscopy (AFM) surface roughness measurements showed for all SiO_2 thin films lower values with a minimum of 4.9 nm (RMS), compared to 7 nm on Si. The electrical film resistivity was determined on SiO_2 with CTLM analysis, depending on the process gas composition. The gained knowledge is beneficial for MEMS applications, where tailored 3C-SiC-on-SiO_2 structures are desired. [2024-0114]**

***Index Terms*— 3C-SiC, alternating supply deposition, LPCVD, silicon carbide, SiO_2.**

I. Introduction

DURING the early stages of CMOS scaling, the importance of engineered substrates gained significant interest. One key parameter was understanding the interface interaction between sublayers [1]. Without this innovation the rapid progress of doubling the possible numbers of transistors in an integrated circuit every two years, described by Moore's law, would not have been possible [2], [3]. In addition to the field of microelectronics, engineered substrates such as *silicon-on-insulator* (SOI) wafers are of utmost importance for microelectromechanical system (MEMS) devices, such as resonators [4], [5], [6], [7], [8], [9], [10], [11], [12] or membrane-based architectures [13], [14], [15], [16]. However, silicon (Si) suffers from electrical instability at ambient temperatures of 250 °C for electronic devices [17], [18], [19]. SiC is known as a wide band gap material with 2.29 to 3.3 eV [20], [21] and features a high breakdown electric field strength of 3 – $4{\cdot}10^6$ V/cm compared to Si ($2{\cdot}10^5$ V/cm) [17], making it suitable for high-power applications at elevated temperatures. Additionally, above temperatures of 500 °C Si loses its mechanical reliability for structural applications [22], [23]. Therefore, the approach of *silicon carbide on insulator* (SiCOI) [24], [25], [26], [27], [28] has been developed already 25 years ago. The improvement of the temperature related mechanical stability over 350 °C [19], [22], hardness of 20.9 GPa [29], [30], mechanical strength of 185 GPa [31], [32], [33] compared to Si and combined with the excellent chemical inertness [34], makes SiC an outstanding candidate for high-temperature applications. Although over 280 polytypes are known for SiC, only the cubic 3C-SiC can be synthesized at process temperatures below 1400 °C making it suitable for depositions on Si or SiO_2 composite substrates [35], [36]. As many MEMS devices are not restricted to single crystalline materials, polycrystalline 3C-SiC is regarded as a suitable material for structural applications.

In this paper we present results on polycrystalline 3C-SiC thin films deposited with LPCVD on thermally grown silicon dioxide (SiO_2) on Si. Studies of 3C-SiC-on-SiO_2 can already be found in the literature, where traditional simultaneous supply depositions (SSD) were employed [37], [38], [39], [40], [41]. Nevertheless, we employed for the first time the alternating supply deposition (ASD) technique [42], [43], [44], [45], [46] on SiO_2 as a special type of pulsed CVD. We already showed in a previous study, that with ASD it is possible to specifically tailor the coefficient of thermal expansion (CTE) of 3C-SiC thin films in a range from 4.37 ppm/K to 13.96 ppm/K [47]. Additionally, ASD claims to yield 3C-SiC thin films featuring both lower full width at half maximum (FWHM) when evaluating X-ray diffraction (XRD) rocking curves and smoother surfaces [45]. This study will show, that we are able to fabricate 3C-SiC thin films on SiO_2 with tailored characteristics such as growth rate, surface roughness, grain size and electrical conductivity solely controlled with the process gas flow rates. We will provide knowledge on the growth mechanism on SiO_2 and discuss substantial differences and similarities of 3C-SiC films deposited in parallel on Si. To the best of the authors' knowledge, the deposition of

Received 26 June 2024; revised 28 August 2024; accepted 21 September 2024. Subject Editor P. Feng. *(Corresponding author: Philipp Moll.)*

Philipp Moll, Georg Pfusterschmied, and Ulrich Schmid are with the Institute of Sensor and Actuator Systems (ISAS), TU Wien, 1040 Vienna, Austria (e-mail: philipp.moll@tuwien.ac.at; georg.pfusterschmied@tuwien.ac.at; ulrich.e366.schmid@tuwien.ac.at).

Sabine Schwarz is with the Service Unit of University Service Centre for Transmission Electron Microscopy (USTEM), TU Wien, 1040 Vienna, Austria (e-mail: sabine.schwarz@tuwien.ac.at).

Werner Artner is with the Service Unit of X-Ray Center (XRC), TU Wien, 1040 Vienna, Austria (e-mail: werner.artner@tuwien.ac.at).

Color versions of one or more figures in this article are available at https://doi.org/10.1109/JMEMS.2024.3472286.

Digital Object Identifier 10.1109/JMEMS.2024.3472286

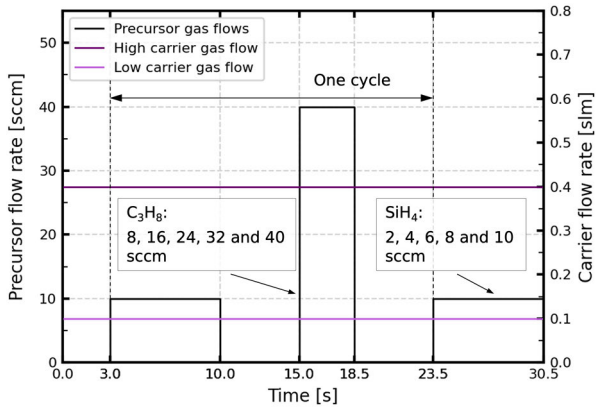

Fig. 1. Schematic representation of one full ASD deposition cycle. The flow rates of the precursors were set 2, 4, 6, 8 and 10 sccm for SiH_4 and 8, 16, 24, 32 and 40 sccm for C_3H_8, whereas the ratio of SiH_4 to C_3H_8 was always set to 1/4.

3C-SiC thin films on SiO_2 using ASD is not reported in the literature so far.

II. Experimental Details

As SiO_2 substrates we used 4 " Si <100> wafers with a 250 nm LPCVD grown oxide on top. For reasons of comparison, we also used pure, n-doped 4 " Si <100> and <111> wafers with a bulk conductivity of 50 Ω·cm. As LPCVD furnace we utilized an EasyTube 3000EXT industrial quartz oven from FirstNano. More details on the LPCVD equipment can be found elsewhere [48]. The basic deposition process consists of three parts. First, all samples were treated with a hydrogen (H_2) *in situ* cleaning step at 1000 °C with 5 slm for 10 minutes at atmospheric pressure. Subsequently, a tailored fast carbonization step was applied [49], [50], [51], [52] to overcome the lattice mismatch of ∼20 % [35], [53] and passivate the Si surface against thermal hydrogen etching [54]. Hereby, the furnace ramps up from 900 °C to 1085 °C in 20 minutes with 1 slm of H_2 and 100 sccm of propane (C_3H_8). After 5.5 minutes at an ambient pressure of 20 torr the formation of the intermediate buffer layer was finished. The third step is the implementation of the ASD synthetization of polycrystalline 3C-SiC. To do so, the precursor gases were introduced successively into the reaction chamber separated by pump-out steps. For the silicon precursor we used pure silane (SiH_4) and for the carbon precursor propane. To achieve a supportive flow regime H_2 was implemented as carrier gas [34], [55]. Figure 1 shows a schematic of one representative ASD cycle. The precursor gases are introduced into the reaction chamber with a ratio of 1/4 for SiH_4/C_3H_8 with flow rates of 2, 4, 6, 8, 10 sccm and 8, 16, 24, 32, 40 sccm for SiH_4 and C_3H_8, respectively. For the carrier gas, flow rates of $\Psi_{low} = 0.1$ slm and $\Psi_{high} = 0.4$ slm of H_2 were investigated.

During all depositions the temperature of 1000 °C and the pressure of 0.32 torr were constant. In a first step we determined the growth per cycle on all substrates to achieve in a second step comparable layer thicknesses of 400 nm ± 5 % for thin film characterization. To investigate the growth behavior, we deposited on each substrate type thin films with 10, 30, 60, 90 and 120 cycles and process gas flows of 10 sccm for SiH_4 and 40 sccm for C_3H_8 with Ψ_{high}. For better readability and due to the frequent occurrence of this gas flow combination, the parameter Ψ_A is introduced. The layer thickness was optically measured utilizing a Filmetrics F20-UVX thin film analyzer within a wavelength range from 600 nm to 1600 nm. For cross-sectional scanning electron measurements (SEM) recordings a Hitachi SU8030 scanning electron microscope with an acceleration voltage of 4 kV was used. For chemical analysis the samples were investigated with X-ray photoelectron spectroscopy (XPS) depth profiling, utilizing a SPECS XP-spectrometer equipped with a monochromatic Al-Kα X-ray source and a hemispherical WAL-150 analyzer. The crystallographic orientation of the thin films was determined with X-ray diffraction (XRD) measurements with a Malvern PANalytical X'pert PRO X-ray powder diffractometer. The measurements were taken at 45 kV and 40 mA with a copper Kα radiation source. Diffraction patterns in Bragg-Brentano configuration were performed from $2\theta = 15$ ° to 90 ° and rocking curves were taken in the range from 34 ° to 38 °, since the most prominent 3C-SiC peak was expected at around 36 ° [39]. To quantitatively assess the preferred crystallographic growth orientation, we employed the texture coefficient (TC) calculation using the Harris method outlined in [56]

$$TC_{(hkl)} = \frac{I_{m(hkl)}/I_{0(hkl)}}{\left(\frac{1}{n}\right)\sum\left[I_{m(hkl)}/I_{0(hkl)}\right]}. \quad (1)$$

Here, the term *(hkl)* refers to the specific growth plane under examination, I_m denotes the normalized measured intensity with the background intensity subtracted, I_0 represents the intensity of a randomly oriented polycrystalline sample sourced from a Powder Diffraction File (PDF) card and n gives the number of planes analyzed. The PDF card utilized in this study for 3C-SiC was #00-029-1129 and the crystallographic planes investigated for TC calculation were (111), (200), (220) and (311) resulting in $n = 4$.

We performed AFM measurements on sample areas of 3×3 μm^2 to determine the surface roughness with a Bruker Dimension Edge atomic force microscope in tapping mode, with a NHCV-tip (spring constant ∼40 N/m). HRTEM and electron diffraction investigation on the Si/3C-SiC and SiO_2/3C-SiC interfaces were performed with a TECNAI F20 transmission electron microscope operating with an acceleration voltage of 200 kV.

For the electrical characterization of the unintentionally doped 3C-SiC thin films circular transmission line method (CTLM) analysis were performed to determine the film resistivity ρ and the specific contact resistance ρ_C, according to the model of Klootwijk and Timmering [57]. I/V (current/voltage)-curves for each gas flow composition were recorded, whereas the SiO_2 served as an electrical insulating layer to the Si substrate. The contact pads were fabricated with a reverse sputter lift off process consisting of 15 nm of titanium (Ti) and 100 nm of tantalum (Ta) with no post deposition annealing. Following [57], ten contact pads per sample were designed with the shape of two concentrical circles forming a center electrode with a radius of 200 μm and an accompanying outer electrode with an inner radius ranging from 220 to 400 μm.

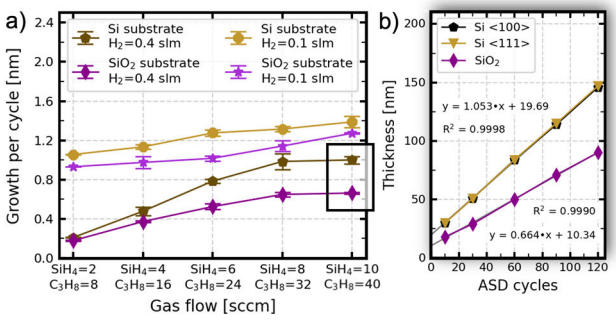

Fig. 2. Growth per cycle of polycrystalline 3C-SiC thin films deposited with increasing precursor gas supply and two different carrier gas flows on Si and SiO_2 substrates can be seen in a). The layer thickness was measured in the middle of the sample. Depositions of five Ψ_A thin films with 10, 30, 60, 90 and 120 cycles on <100> Si, <111> Si and SiO_2 are presented in b). A linear increase in layer thickness on all substrates can be seen, whereas the growth per cycle on both silicon substrates was almost identical, while the growth rate for SiO_2, however, was significant lower.

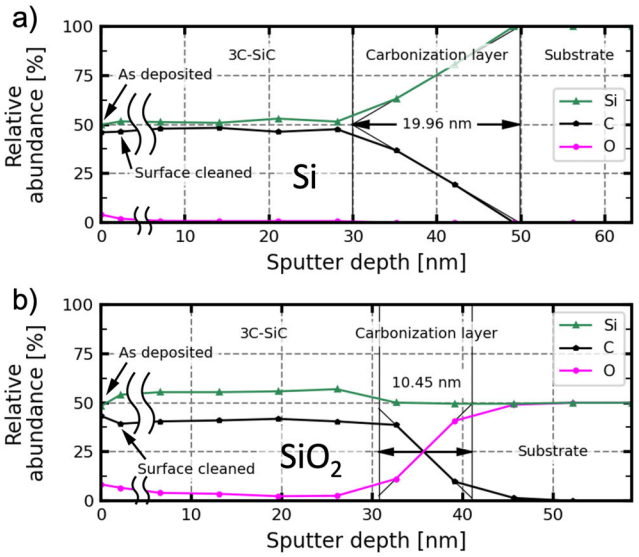

Fig. 3. XPS depth profiling showing the relative presence of Si, C and O through a 3C-SiC cross section. In a) the element analysis of the 3C-SiC/Si interface can be seen. With a depth resolution of ∼7 nm, a carbonization layer thickness of ∼20 nm was measured. The depth profile of b) gives the chemical composition around the 3C-SiC/SiO_2 interface. The main differences between both measurements are a smaller carbonization layer thickness of ∼10 nm (with ∼6.5 nm resolution) and an oxygen proportion of 7.5 % through the whole thin film.

The I/V curves for the CTLM analysis were taken with a Süss PM8 waferprober and an Agilent B2911A Precision Source/Measure Unit from −3 V to 3 V in 61 steps.

III. Results

To start, the growth per cycle for different process gas flow rates is presented in Figure 2 a). Regardless of the substrate type the growth per cycle was lower for Ψ_{high}. This finding originates from the nature of the ASD deposition scheme, where at each cycle first an ultra-thin silicon layer is deposited, followed by a carbon-assisted silicon redistribution, thus forming 3C-SiC [48]. During deposition this thin silicon layer is attacked by the hydrogen gas, hence reducing the growth per cycle, when using higher H_2 flow rates. This influence is well-known in silicon technology as hydrogen thermal etching [54]. Simultaneously, hydrogen passivation [58] and inhibition-effect [59], [60], [61] takes place, both contributing in a decreased growth per cycle. This entails the saturation of surface defects or Si dangling bonds with hydrogen atoms and interactions with the Si surface, thus reducing the reactivity of the Si and inhibit the adsorption and incorporation of C precursors. This stands in contrast with SSD depositions where increased growth rates are typically observed with higher H_2 flow rates. For Ψ_{low} depositions a linear dependency as a function of the precursor flow rates was measured. For Ψ_{high} depositions, however, when exceeding a threshold of 8 sccm for SiH_4 and 32 sccm for C_3H_8 the growth per cycle saturated. Since the growth per cycle did not further increase by providing even more precursor gases this saturation effect is explained by a reaction limited process [62].

The main difference visible in Figure 2 a) is that for the same deposition conditions the growth per cycle was always lower on SiO_2, than on Si. Very little can be found in the literature, when it comes to LPCVD growth rates on SiO_2 compared to Si [37]. To clarify the origin of the difference in growth per cycle we present the thickness of different depositions with increasing number of ASD cycles on <100> Si, <111> Si and SiO_2, which is illustrated in Figure 2 b). The two Si samples showed identical results and a highly linear growth behavior with a measured growth per cycle rate of 1.05 nm. We also found a highly linear growth behavior for SiO_2, however, with a lower growth per cycle of 0.66 nm. Both rates correspond to what is presented in Figure 2 a) for the Ψ_A deposition (black box). Additionally, the two calculated intercepts with the y-axis represents the thickness of the carbonization layer resulting in 19.69 nm and 10.34 nm for Si and SiO_2, respectively. Two hypotheses seem reasonable for an inhibited growth behavior on SiO_2: first, the amorphous seed layer is disadvantageous for 3C-SiC crystal growth. This can be motivated, since amorphous substrates lack of a crystalline structure, which can hinder the nucleation and growth of 3C-SiC compared to single crystal Si, thus resulting in reduced growth rates and lower thin film quality. Second, oxygen effusion from the SiO_2 surface prevents the crystal growth compared to Si.

To further investigate this hypothesis, we performed XPS depth-profiling. Two representative measurements of the same Ψ_A deposition on Si and SiO_2 are shown in Figure 3. All thin films grown on SiO_2 exhibit an oxygen content of 7.5 ± 2.5 % through the whole thin film, compared to <1 % on Si. The homogeneous distribution of oxygen throughout the entire thin film can be explained by vacancy diffusion [63], [64]. Eickhoff et al. [37] showed, that at elevated temperatures above 1150 °C SiO_2 substrates reach up to 100 % selectivity during 3C-SiC CVD depositions compared to pure Si surfaces. It is also shown that for lower temperatures the growth rate is decreased compared to Si.

This indicates that the oxygen inhibits the growth of 3C-SiC. Even more, Nagasawa and Yagi state, that in their studies even the thinnest SiO_2 layers prevent the surface from chemically adsorbing the carbon precursor [65]. We propose, that the

oxygen present within the thin films partially forms SiO_2 during each SiH_4 ASD sequence, thus inhibiting the carbon to react with the silicon and hence decreasing the growth per cycle. This assumption is also in line with the lower thickness of the carbonization layer on SiO_2 since the oxygen lowers the adsorption of the carbon during the carbonization step.

Thus, only a ∼10 nm thin carbon layer is deposited on the surface. Furthermore, XPS measurements revealed, that all thin films deposited on Si are confirmed to be stoichiometric, whereas thin films deposited on SiO_2 turned out to be non-stoichiometric with a higher percentage of Si content.

Figure 4 shows the XRD spectra of the different 3C-SiC films on both substrates, whereas the most prominent peak was measured at 35.78 °, which can be attributed to the <111> direction. With the other peaks detected at 41.48 ° and 60.1 °, which can be assigned to the <200> and <220> directions, we conclude that the thin films consist only of poly 3C-SiC. One representative rocking curve for each substrate is shown in the inserts of Figure 4, with the lowest full width at half maximum (FWHM) values at 1.112 ° and 0.446 ° for Si and SiO_2, respectively. For both substrates the Ψ_A gas flow configuration resulted in the lowest FWHM results. Typical values for comparable poly 3C-SiC thin films on Si are in the range of 1.4 ° to 1 ° [43]. For SiO_2, however, no similar study could be found to compare our results.

The texture coefficient, presented in Figure 4 b) and d), revealed only for Ψ_{high} depositions on SiO_2 a preferred growth orientation in the (111) plane. Other gas flow combinations did not exhibit a preferred growth orientation. The reason for the prominent formation of <111> 3C-SiC on the SiO_2 is because of the low free surface energy of <111> facets, which tend to form <111> 3C-SiC even on amorphous surfaces [39]. This phenomenon is well-documented in the literature for 3C-SiC depositions [40], [66], [67], [68], despite the fact that the <110> direction exhibits an even lower surface energy of 3.4 J/m^2 compared to the 4.2 J/m^2 of the <111> direction [69]. On single crystal substrates the deposited thin films tend to grow in the same direction as the seed crystal [67]. It is also reported, that if the growth direction of the thin film deviates from the substrate orientation, two explanations can be given. First, because of a higher density of aligned atoms per unit, forming a more stable thin film [70]. For example, the density of aligned atoms per unit of <111> 3C-SiC on <110> Si is 4 times higher than <110> 3C-SiC on <110> Si, thus forming a thin film, where the <111> direction is preferred [67], [70]. The second opinion proposed by Zheng et al. is the impact of the carbonization layer [67].

For better understanding of the XRD results we took HRTEM recordings of the 3C-SiC/Si and 3C-SiC/SiO_2 interfaces, presented in Figure 5 a) and b). Electron diffraction patterns of the two substrates and the corresponding 3C-SiC thin films are presented in the section e) – h) of Figure 5. The Si diffraction pattern shows a single crystal pattern with a lattice constant of $d_{111} = 3.123$ Å almost matching the lattice constant of a stress-free Si crystal with $d_{111} = 3.136$ Å [53]. As expected, an amorphous pattern was recorded for the SiO_2 substrate. The diffraction patterns for the thin films confirm a polycrystalline microstructure in the investigated regions. Thin

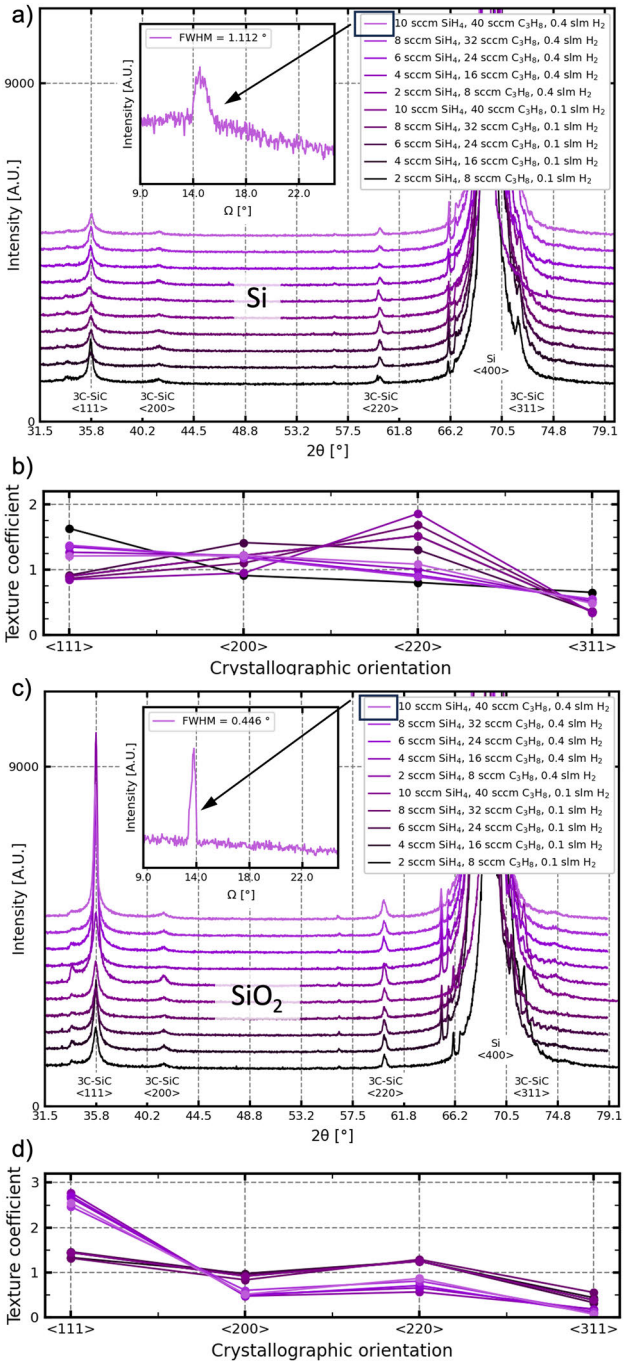

Fig. 4. XRD measurements of the 3C-SiC thin films investigated in this study, while a) gives the results on Si [48], and c) those on SiO_2. Most prominent in both diagrams is the <111> of 3C-SiC at 35.79 °. Both, in a) and c) the inserts show the rocking curves with the lowest FWHM values. The TC was calculated for each crystallographic plane, illustrated for Si in b) and SiO_2 in d).

films grown on Si, however, show streaks at the diffraction spots, indicating higher strain levels, compared to those grown on SiO_2.

Electron energy loss spectroscopy (EELS) measurements [48] of the 3C-SiC/Si interface revealed that the carbonization layer consists of a 3 – 6 nm carbonized Si section, followed by a 10 – 15 nm amorphous carbon layer, on top the 3C-SiC thin film. This means that the thin films grow on an amorphous carbon seed layer when using Si as

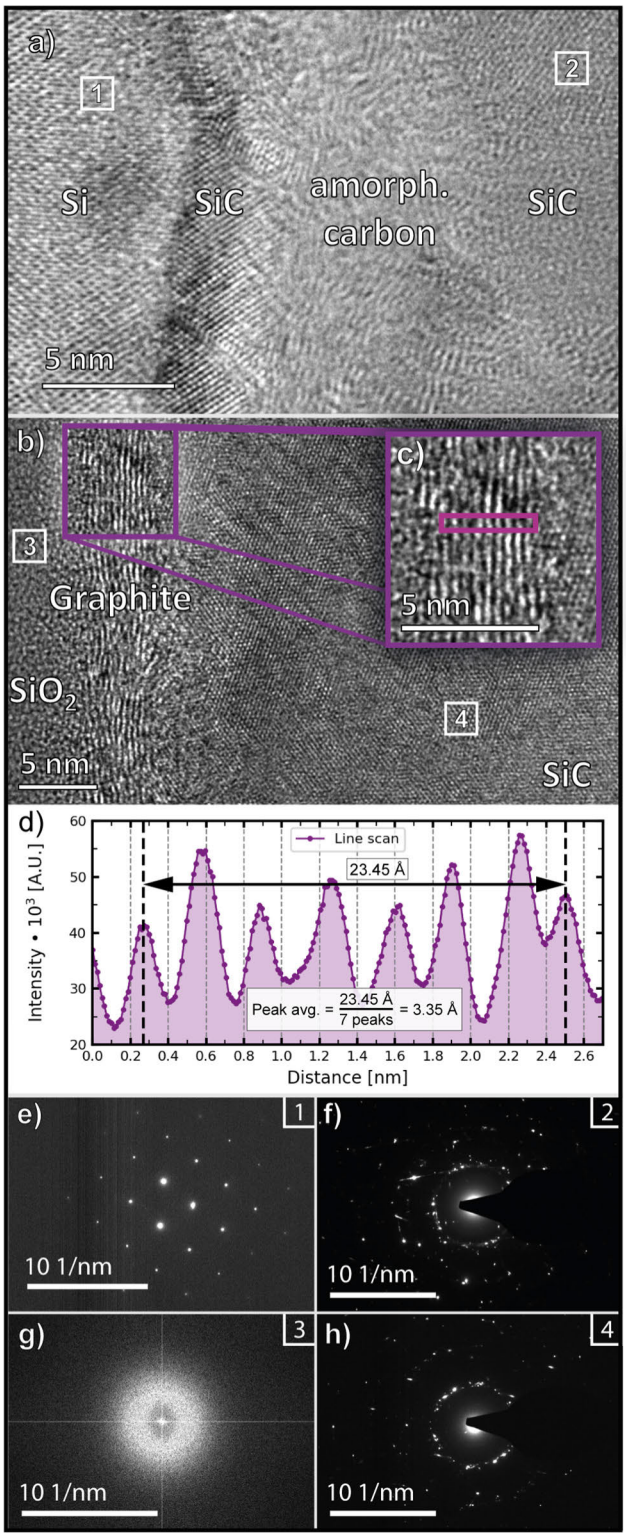

Fig. 5. In a) a HRTEM of the carbonization layer on Si can be seen. For comparison the carbonized interface of the SiO_2 substrate with 3C-SiC on top is presented in b) and with higher magnification in c). A 2.7 nm long intensity profile of the graphitic layer is depicted in d). The position, where the profile was conducted is highlighted in Figure 5 c).The electron diffraction patterns from d) – g) depict the regions of pure Si, 3C-SiC grown on Si, pure SiO_2 and 3C-SiC grown on SiO_2, respectively.

substrate, explaining the most prominently <111> crystallographic orientation of the poly 3C-SiC. The resemblance of the XRD results on both Si and SiO_2 substrates is explained

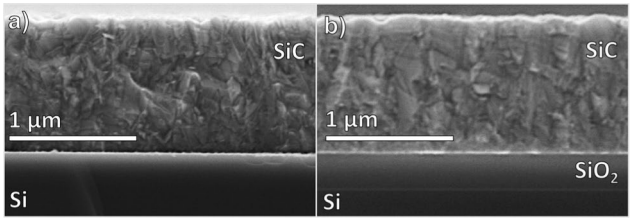

Fig. 6. Similar 3C-SiC thin film microstructures on Si and SiO_2 visualized by cross-sectional SEM recordings as illustrated in a) and b). For reasons of comparison a desired layer thickness of 1 μm was achieved with 1050 and 1500 cycles for Si and SiO_2, respectively.

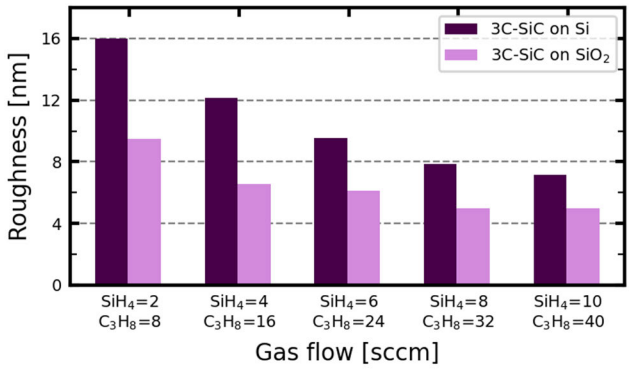

Fig. 7. Comparison of the surface roughness of representative Ψ_{high} thin films with a thickness of 400 nm ± 5 % deposited on Si and SiO_2 as a function of the precursor flow rate.

by the excess carbon at the interface originated from the carbonization step. The smaller FWHM results from a crystalline graphite carbonization layer. This graphitic layer was confirmed by an intensity profile of the HRTEM, as highlighted in Figure 5 c). The lattice plane distance d_{200} was determined with 3.35 Å ± 0.03 Å, as shown in Figure 5 d). This result is in perfect agreement with similar studies [71] and to what is provided for graphite lattice distances in XRD studies [72], [73]. On Si, however, the carbonization step resulted in an amorphous carbon layer, thus providing less vital conditions for the deposition of high-quality 3C-SiC thin films. It can be concluded that the choice of an individual carbonization step for each substrate is crucial. The values for the carbonization layer thickness determined from the growth rate (see Figure 2 b) and the measured thickness of the XPS depth-profiling are in good agreement with the corresponding value from the HRTEM analysis. Even more, it is in good agreement to data in the literature [45], [49], [74].

The SEM analysis of the 3C-SiC thin films on Si and SiO_2, given in Figure 6a) and b), show comparable cross-sections. This can be explained by the excess carbon from the carbonization step, resulting in similar microstructures for all 3C-SiC thins films independent of the substrate type.

The results from AFM surface roughness measurements were set in relation with the corresponding layer thickness and are illustrated in Figure 7. At a comparable film thickness, a smoother surface topography is measured on all SiO_2 samples compared to Si. For both substrates a decreasing trend was measured for the RMS roughness, whereas independent from the carrier flow rate, smoothest surfaces can be contributed to

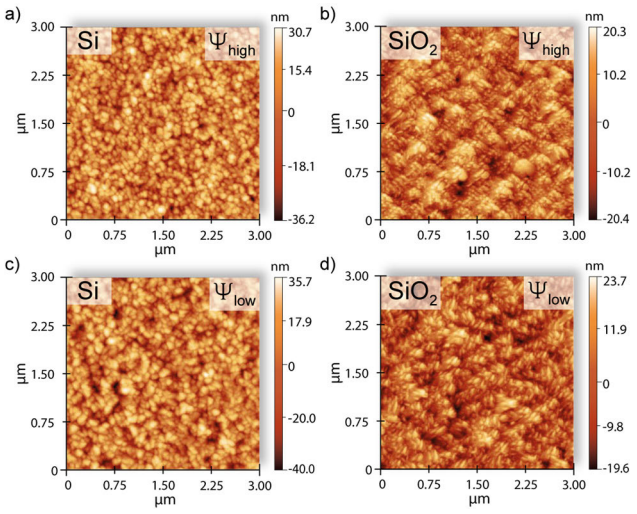

Fig. 8. Representative AFM pictures taken from depositions with 10 sccm for SiH_4 and 40 sccm for C_3H_8 with Ψ_{high} can be seen in a) and b) and with Ψ_{low} in c) and d). The left column shows typical spherical shaped grain patterns on Si, whereas in the right column different results on SiO_2 can be seen. (Note: the pictures for Si and SiO_2 were taken consecutively for every precursor and carrier gas flow to avoid any doubts in the correctness of the measurements.)

the highest precursor flow rates. This can be explained by the inhibiting hydrogen effects, influencing not only the growth rate, but also affecting the surface roughness by extensive hydrogen exposure. Lowest values for the RMS roughness of 4.9 nm were measured on SiO_2 at a 3C-SiC film thickness of about 400 nm. In literature, most values for SiO_2 can be found around 20 nm for the RMS roughness for thicknesses >2 μm, whereby also mirror-like surfaces with 3 – 5 nm can be achieved with special post-deposition treatments (*e.g.* polishing) [39], [40], [41]. In addition, we achieved for thin films deposited on Si, mirror-like surfaces [68] with an RMS roughness below 7 nm. For 3C-SiC thin films on Si substrates a broad range is reported for this parameter in the literature ranging from 3 nm at ∼400 nm [43] up to 60 nm, strongly dependent on the layer thickness, the process gases, pressures or deposition regimes [43], [68], [75]. Not only smoother surfaces were measured on SiO_2, also different patterns for the surface topography were recorded by AFM measurements, as shown in Figure 8. For the Si depositions we achieved typical patterns for the grain structure, comparable to what can be found in the literature [39], [68], [76]. On SiO_2, however, the ASD thin films revealed a completely different topology. The 3C-SiC-on-SiO_2 topology of this study cannot be compared to SSD depositions on SiO_2, where the grains exhibit a spherical shape and are indistinguishable from those on Si substrates [39], [77], [78], [79]. We propose that the variance between the two topographies of Si and SiO_2 depositions is also a result of the oxygen within the SiO_2 thin films.

Typical I/V measurements, as illustrated in Figure 9, provide an overview on the electrical properties of the investigated undoped 3C-SiC thin films as a function of the precursor flow rate. The Ti/Ta contact pads show perfect ohmic behavior within the investigated voltage range without the need for an annealing step.

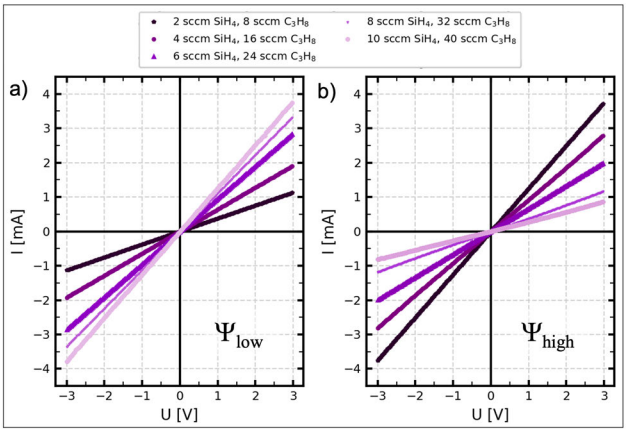

Fig. 9. I/V curves from undoped poly 3C-SiC thin films depending on the process flow rates. The I/V curves were measured on the contact pad with a spacing of 200 μm between the electrodes.

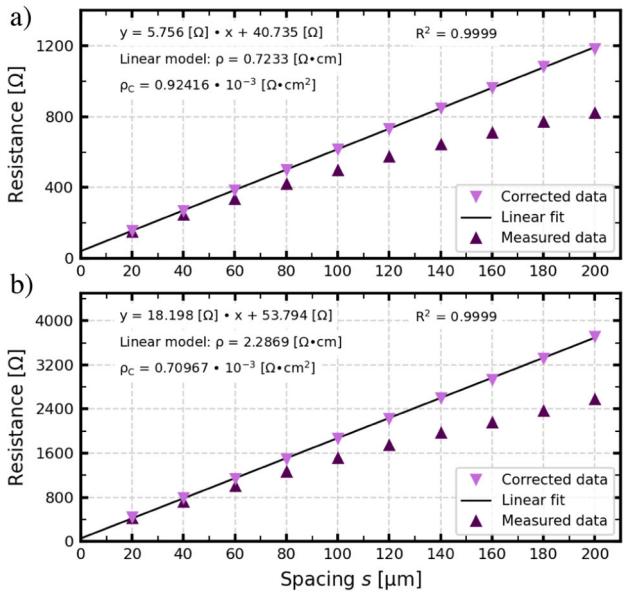

Fig. 10. Representative CTLM measurements for the lowest and highest total resistance, presented in a) and b) corresponding to the flow rates of 2 sccm SiH_4 and 8 sccm C_3H_8, and 10 sccm SiH_4 and 40 sccm C_3H_8, both deposited with Ψ_{high}.

Two opposing trends can be seen for each of the carrier flow rate. While for Ψ_{low} the total resistance R decreases with increasing precursor flow rate, while for Ψ_{high} R decreases with decreasing precursor flow rate. Two examples, representing the highest and lowest resistance, are employed to illustrate the evaluation of the CTLM analysis, presented in Figure 10. The total resistances measured for each CTLM contact pad are plotted as a function of the corresponding spacings and a linear approximation is introduced, using a geometrical correction factor [57]. From the slope of the curve, the dimensions of the contacts and the film thickness, the film resistivity can be determined. The contact resistance R_C and the specific contact resistance ρ_C are determined from the intersections of the linear approximation with the x- and y-axes, respectively.

The results from the CTLM analysis are illustrated in Figure 11. For Ψ_{low} depositions decreasing resistivities with increasing precursor flow rates from 2.11 to 0.74 Ω·cm were measured. The resistivities for Ψ_{high} were in the same range

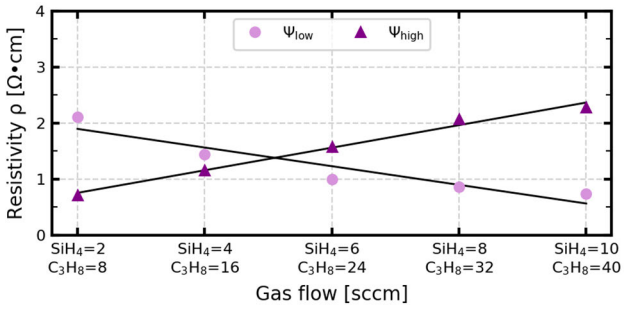

Fig. 11. Film resistivity of undoped 3C-SiC thin films as a function of the process gas flow rates, derived from CTLM analysis.

from 2.28 to 0.72 Ω·cm, however, as a result of decreasing precursor flow rates. Strongly depending on the carbonization step, resistivities for undoped poly 3C-SiC thin films in the range of about 1 up to 6600 Ω·cm can be achieved [1]. The contact resistances R_C showed no dependency on the gas flow rates and were in the range of 15 to 27 Ω, resulting in specific contact resistances ρ_C ranging from $7.1{\cdot}10^{-4}$ to $1.27{\cdot}10^{-3}$ Ω·cm^2.

Comparable undoped 3C-SiC thin films exhibit values for ρ_C in the range of $5{\cdot}10^{-4}$ to $1.2{\cdot}10^{-5}$ Ω·cm^2 [80], [81], [82]. In general, electron scattering at grain boundaries can be named as the main phenomenon influencing the resistivity in unintentionally doped polycrystalline thin films [83], together with the incorporation of nitrogen atoms [84]. Taking this into account and the characteristic of an ideal SiC bulk crystal being electrically insulating at room temperature, it can be concluded that the two thin films showing the highest film resistivity (Ψ_{low}: 2 sccm for SiH_4, 8 sccm for C_3H_8 and Ψ_{high}: 10 sccm for SiH_4, 40 sccm for C_3H_8), exhibit lowest impurity levels and lowest grain boundary density. This is in good agreement with the XRD results, where the two abovementioned gas flow compositions achieved lowest FWHM values. Both thin films originated from a balanced carrier to precursor gas flow ratio (low carrier flow rate – lowest precursor flow rate and high carrier flow rate – highest precursor flow rate), whereby the resistance as well as the FWHM of the other thin films increased the more unbalanced this ratio becomes. It is worth noting that the grow-inhibiting hydrogen effects dominate the thin film characteristics, thus influencing the film resistivity depending on the process gas flows.

IV. Conclusion

In this study we demonstrated the deposition of 3C-SiC on SiO_2 using ASD in a LPCVD system. By comparing the growth per cycle of the same depositions on Si we measured an inhibited growth behavior on SiO_2. XPS depth profiling revealed an increased oxygen content of 7.5 % throughout the entire thin film grown on SiO_2. The elevated oxygen level could potentially explain the decreased growth per cycle. On both substrates typical poly 3C-SiC XRD patterns were measured, whereas the <111> peak appeared as the most prominent crystallographic orientation. Hereby Ψ_{high} depositions on SiO_2 exhibited a preferred growth orientation in the <111> direction. The HRTEM analysis revealed an amorphous carbon layer on top of the carbonized Si substrate. On the SiO_2 interface, however, a graphite layer was found, providing an explanation for lower FWHM values for the 3C-SiC thin films. This indicates the outstanding importance of tailored carbonization steps for each substrate. Nevertheless, the excess carbon at both interfaces provides comparable growth conditions, therefore explaining the highly <111> textured thin films with similar microstructure verified with cross-section analyses on both substrates. From AFM measurements we found smoother surfaces for SiO_2, with a minimum of 4.9 nm for the RMS roughness, whereas also different surface topologies were recorded. For both substrates the RMS roughness decreased with increasing precursor flow rate.

CTLM measurements showed the importance of the ratio from carrier to precursor gas flow rates. Hereby, Ψ_{low} paired with lowest precursor flow rates of 2 sccm for SiH_4 and 8 sccm for C_3H_8 as well as Ψ_{high} with 10 sccm SiH_4 and 40 sccm C_3H_8 achieved highest film resistivities of ∼2.3 Ω·cm, giving strong indication of a lower impurity as well as grain boundary density values compared to thin films deposited with other gas flow compositions. This is consistent with the XRD rocking curve results, whereas lowest FWHM values were achieved by the above-mentioned well-balanced ratios of the process gas flow rates. The results in this study provide knowledge to achieve tailored thin film properties, enabling customized fabrication of improved SiCOI structures for MEMS applications.

References

[1] P. Moll, G. Pfusterschmied, and U. Schmid, "Impact of excess carbon at the 3C-SiC/SiO_2 interface using LPCVD-based alternating supply deposition," in *Proc. IEEE 37th Int. Conf. Micro Electro Mech. Syst. (MEMS)*, Jan. 2024, pp. 606–609.

[2] E. A. Fitzgerald, "Engineered substrates and their future role in microelectronics," *Mater. Sci. Eng., B*, vols. 124–125, pp. 8–15, Dec. 2005.

[3] G. E. Moore, "Cramming more components onto integrated circuits," *Proc. IEEE*, vol. 86, no. 1, pp. 82–85, Jan. 1998.

[4] S. Alasatri, M. Schneider, J. Mirwald, B. Hofko, and U. Schmid, "Accuracy and precision of resonant piezoelectric MEMS viscosity sensors in highly viscous bituminous materials," *Sens. Actuators A, Phys.*, vol. 347, Nov. 2022, Art. no. 113903.

[5] L. Belsito, M. Bosi, F. Mancarella, M. Ferri, and A. Roncaglia, "Nanostrain resolution strain sensing by monocrystalline 3C-SiC on SOI electrostatic MEMS resonators," *J. Microelectromech. Syst.*, vol. 29, no. 1, pp. 117–128, Feb. 2020.

[6] S. Fei and H. Ren, "Temperature characteristics of a contour mode MEMS AlN piezoelectric ring resonator on SOI substrate," *Micromachines*, vol. 12, no. 2, p. 143, Jan. 2021.

[7] M. Kucera et al., "Characterisation of multi roof tile-shaped out-of-plane vibrational modes in aluminium-nitride-actuated self-sensing micro-resonators in liquid media," *Appl. Phys. Lett.*, vol. 107, no. 5, Aug. 2015, Art. no. 053506.

[8] J. E.-Y. Lee, J. Yan, and A. A. Seshia, "Study of lateral mode SOI-MEMS resonators for reduced anchor loss," *J. Micromech. Microeng.*, vol. 21, no. 4, Apr. 2011, Art. no. 045010.

[9] X. Liu, L. P. B. Katehi, W. J. Chappell, and D. Peroulis, "High-Q tunable microwave cavity resonators and filters using SOI-based RF MEMS tuners," *J. Microelectromech. Syst.*, vol. 19, no. 4, pp. 774–784, Aug. 2010.

[10] G. Pfusterschmied, F. Patocka, C. Weinmann, M. Schneider, D. Platz, and U. Schmid, "Responsivity and sensitivity of piezoelectric MEMS resonators at higher order modes in liquids," *Sens. Actuators A, Phys.*, vol. 295, pp. 84–92, Aug. 2019.

[11] G. Pfusterschmied et al., "Potential of piezoelectric MEMS resonators for grape must fermentation monitoring," *Micromachines*, vol. 8, no. 7, p. 200, Jun. 2017.

[12] G. S. Wood, C. Zhao, S. H. Pu, S. A. Boden, I. Sari, and M. Kraft, "Mass sensor utilising the mode-localisation effect in an electrostatically-coupled MEMS resonator pair fabricated using an SOI process," *Microelectron. Eng.*, vol. 159, pp. 169–173, Jun. 2016.

[13] M. Schneider, M. Dorfmeister, P. Moll, M. Kaltenbacher, and U. Schmid, "Bi-stable aluminum nitride-based piezoelectric micromachined ultrasonic transducer (PMUT)," *J. Microelectromech. Syst.*, vol. 29, no. 5, pp. 948–953, Oct. 2020.

[14] P. Moll et al., "Biocompatible a-SiC:H-based bistable MEMS membranes with piezoelectric switching capability in fluids," *J. Microelectromech. Syst.*, vol. 31, no. 3, pp. 372–383, Jun. 2022.

[15] M. Dorfmeister, B. Kössl, M. Schneider, G. Pfusterschmied, and U. Schmid, "Switching performance of bistable membranes activated with integrated piezoelectric thin film transducers," *J. Micromech. Microeng.*, vol. 29, no. 10, Oct. 2019, Art. no. 105008.

[16] X. Miao, X. Dai, Y. Huang, G. Ding, and X. Zhao, "Large out-of-plane displacement bistable electromagnetic microswitch on a single wafer," *Sensors*, vol. 16, no. 5, p. 634, May 2016.

[17] M. Bhatnagar and B. J. Baliga, "Comparison of 6H-SiC, 3C-SiC, and Si for power devices," *IEEE Trans. Electron Devices*, vol. 40, no. 3, pp. 645–655, Mar. 1993.

[18] J. Millán, P. Godignon, X. Perpi na, A. Pérez-Tomás, and J. Rebollo, "A survey of wide bandgap power semiconductor devices," *IEEE Trans. Power Electron.*, vol. 29, no. 5, pp. 2155–2163, May 2014.

[19] H. Lee, V. Smet, and R. Tummala, "A review of SiC power module packaging technologies: Challenges, advances, and emerging issues," *IEEE J. Emerg. Sel. Topics Power Electron.*, vol. 8, no. 1, pp. 239–255, Mar. 2020.

[20] S. Nakashima and M. Hangyo, "Raman intensity profiles and the stacking structure in SiC polytypes," *Solid State Commun.*, vol. 80, no. 1, pp. 21–24, Oct. 1991.

[21] R. K. Willardson and E. R. Weber, *SiC Materials and Devices*. Amsterdam, The Netherlands: Elsevier, 1998.

[22] P. French, G. Krijnen, and F. Roozeboom, "Precision in harsh environments," *Microsyst. Nanoeng.*, vol. 2, no. 1, p. 16048, Oct. 2016.

[23] M. Mehregany and C. A. Zorman, "SiC MEMS: Opportunities and challenges for applications in harsh environments," *Thin Solid Films*, vols. 355–356, pp. 518–524, Nov. 1999.

[24] L. Di Cioccio, F. Letertre, Y. Le Tiec, A. M. Papon, C. Jaussaud, and M. Bruel, "Silicon carbide on insulator formation by the smart-cut process," *Mater. Sci. Eng., B*, vol. 46, no. 1, pp. 349–356, 1997.

[25] Y. Zheng et al., "High-quality factor, high-confinement microring resonators in 4H-silicon carbide-on-insulator," *Opt. Exp.*, vol. 27, no. 9, p. 13053, 2019.

[26] G. H. Kroetz, M. H. Eickhoff, and H. Moeller, "Silicon compatible materials for harsh environment sensors," *Sens. Actuators A, Phys.*, vol. 74, nos. 1–3, pp. 182–189, Apr. 1999.

[27] M. Eickhoff, N. Vouroutzis, A. Nielsen, G. Krötz, and J. Stoemenos, "Oxidation dependence on defect density in 3C-SiC films," *J. Electrochemical Soc.*, vol. 148, no. 6, p. G336, 2001.

[28] G. Krötz et al., "Heteroepitaxial growth of 3C-SiC on SOI for sensor applications," *Mater. Sci. Eng., B*, vols. 61–62, pp. 516–521, Jul. 1999.

[29] J. D. Reddy, A. A. Volinsky, C. L. Frewin, C. Locke, and S. E. Saddow, "Mechanical properties of 3C-SiC films for MEMS applications," *MRS Proc.*, vol. 1049, pp. 1–8, Jan. 2007.

[30] B. Bhushan and V. N. Koinkar, "Microtribological studies of doped single-crystal silicon and polysilicon films for MEMS devices," *Sens. Actuators A, Phys.*, vol. 57, no. 2, pp. 91–102, Nov. 1996.

[31] J. Vanhellemont, A. K. Swarnakar, and O. Van der Biest, "Temperature dependent young's modulus of Si and Ge," *ECS Trans.*, vol. 64, no. 11, pp. 283–292, Aug. 2014.

[32] K. Shirai, "Temperature dependence of young's modulus of silicon," *Jpn. J. Appl. Phys.*, vol. 52, no. 8R, Aug. 2013, Art. no. 088002.

[33] M. Pozzi et al., "Mechanical properties of a 3C-SiC film between room temperature and 600 °C," *J. Phys. D, Appl. Phys.*, vol. 40, no. 11, pp. 3335–3342, Jun. 2007.

[34] M. B. J. Wijesundara and R. Azevedo, *Silicon Carbide Microsystems for Harsh Environments*. Cham, Switzerland: Springer, 2011.

[35] S. E. Saddow, *Silicon Carbide Materials for Biomedical Applications*. Oxford, U.K.: Elsevier, 2016.

[36] S. E. Saddow, *Silicon Carbide Biotechnology. A Biocompatible Semiconductor for Advanced Biomedical Devices and Applications*. Oxford, U.K.: Elsevier, 2012.

[37] M. Eickhoff, H. Möller, M. Rapp, and G. Kroetz, "Selective growth of high-quality 3C-SiC using a SiO_2 sacrificial-layer technique," *Thin Solid Films*, vol. 345, no. 2, pp. 197–199, May 1999.

[38] G. Deokar, M. D'Angelo, and C. D. Cavellin, "Synthesis of 3C-SiC nanocrystals at the SiO_2/Si interface by CO_2 thermal treatment," *J. Nanosci. Nanotechnol.*, vol. 11, no. 10, pp. 6–9232, Oct. 2011.

[39] Z. Yong-Mei et al., "Doped polycrystalline 3C-SiC films deposited by LPCVD for radio-frequency MEMS applications," *Chin. Phys. Lett.*, vol. 25, no. 6, pp. 2269–2272, Jun. 2008.

[40] E. Hurtós and J. Rodríguez-Viejo, "Residual stress and texture in poly-SiC films grown by low-pressure organometallic chemical-vapor deposition," *J. Appl. Phys.*, vol. 87, no. 4, pp. 1748–1758, Feb. 2000.

[41] J. Trevino, F. Xiao-An, M. Mehregany, and C. Zorman, "Low-stress, heavily-doped polycrystalline silicon carbide for MEMS applications," in *Proc. 18th IEEE Int. Conf. Micro Electro Mech. Syst.*, Sep. 2005, pp. 451–454.

[42] L. Wang et al., "Growth of 3C–SiC on 150-mm Si(100) substrates by alternating supply epitaxy at 1000 °C," *Thin Solid Films*, vol. 519, no. 19, pp. 6443–6446, Jul. 2011.

[43] L. Wang et al., "Growth mechanism for alternating supply epitaxy: The unique pathway to achieve uniform silicon carbide films on multiple large-diameter silicon substrates," *RSC Adv.*, vol. 6, no. 20, pp. 16662–16667, 2016.

[44] T. Shimizu, Y. Ishikawa, and N. Shibata, "Epitaxial growth of 3C-SiC on thin silicon-on-insulator substrate by chemical vapor deposition using alternating gas supply," *Jpn. J. Appl. Phys.*, vol. 39, no. 6B, p. 617, Jun. 2000.

[45] H. Nagasawa and Y. Yamaguchi, "Atomic level epitaxy of 3C-SiC by low pressure vapour deposition with alternating gas supply," *Thin Solid Films*, vol. 225, nos. 1–2, pp. 230–234, Mar. 1993.

[46] K. Yagi and H. Nagasawa, "3C–SiC growth by alternate supply of SiH_2Cl_2 and C_2H_2," *J. Cryst. Growth*, vol. 174, nos. 1–4, pp. 653–657, Apr. 1997.

[47] P. Moll, G. Pfusterschmied, and U. Schmid, "Robust polycrystalline 3C-Sic-on-Si heterostructures with low CTE mismatch up to 900 °C for MEMS," in *Proc. IEEE 36th Int. Conf. Micro Electro Mech. Syst. (MEMS)*, Jan. 2023, pp. 590–593.

[48] P. Moll, G. Pfusterschmied, S. Schwarz, M. Stöger-Pollach, and U. Schmid, "Impact of alternating precursor supply and gas flow on the LPCVD growth behavior of polycrystalline 3C-SiC thin films on Si," *Sens. Actuators A, Phys.*, vol. 372, Jul. 2024, Art. no. 115376.

[49] M. Bosi et al., "Optimization of a buffer layer for cubic silicon carbide growth on silicon substrates," *J. Cryst. Growth*, vol. 383, pp. 84–94, Nov. 2013.

[50] N. Bécourt, J. L. Ponthenier, A. M. Papon, and C. Jaussaud, "Influence of temperature on the formation by reactive CVD of a silicon carbide buffer layer on silicon," *Wide-Band-Gap Semicond.*, vol. 185, nos. 1–4, pp. 79–84, Apr. 1993.

[51] G. Ferro et al., "Atomic force microscopy growth modeling of SiC buffer layers on Si(100) and quality optimization," *J. Appl. Phys.*, vol. 80, no. 8, pp. 4691–4702, Oct. 1996.

[52] Z. Zhao, Y. Li, Z. Yin, and Z. Li, "Growth of 3C-SiC on Si(100) by LPCVD using a modified process after the clean step," *J. Mater. Sci., Mater. Electron.*, vol. 27, no. 7, pp. 7095–7099, Jul. 2016.

[53] P. Becker, P. Scyfried, and H. Siegert, "The lattice parameter of highly pure silicon single crystals," *Zeitschrift Für Physik B Condens. Matter*, vol. 48, no. 1, pp. 17–21, Aug. 1982.

[54] T. Tezuka et al., "110-facets formation by hydrogen thermal etching on sidewalls of Si and strained-Si fin structures," *Appl. Phys. Lett.*, vol. 92, no. 19, May 2008, Art. no. 191903.

[55] D. Choi, R. J. Shinavski, W. S. Steffier, and S. M. Spearing, "Residual stress in thick low-pressure chemical-vapor deposited polycrystalline SiC coatings on Si substrates," *J. Appl. Phys.*, vol. 97, no. 7, Apr. 2005, Art. no. 074904.

[56] J.-J. Huang, C. Militzer, C. A. Wijayawardhana, U. Forsberg, and H. Pedersen, "Superconformal silicon carbide coatings via precursor pulsed chemical vapor deposition," *J. Vac. Sci. Technol. A*, vol. 41, no. 3, May 2023, Art. no. 030403.

[57] J. H. Klootwijk and C. E. Timmering, "Merits and limitations of circular TLM structures for contact resistance determination for novel III–V HBTs," in *Proc. Int. Conf. Microelectronic Test Struct.*, Mar. 2004, pp. 247–252.

[58] B. Sopori et al., "Hydrogen in silicon: A discussion of diffusion and passivation mechanisms," *Sol. Energy Mater. Sol. Cells*, vols. 41–42, pp. 159–169, Jun. 1996.

[59] M. J. Duchemin, M. M. Bonnet, and M. F. Koelsch, "Kinetics of silicon growth under low hydrogen pressure," *J. Electrochemical Soc.*, vol. 125, no. 4, pp. 637–644, Apr. 1978.

[60] F. Hottier and R. Cadoret, "Surface processes in low pressure chemical vapour deposition," *J. Cryst. Growth*, vol. 52, pp. 199–206, Apr. 1981.

[61] W. Weerts, M. De Croon, and G. Marin, "The Kinetics of the low-pressure chemical vapor deposition of polycrystalline silicon from silane," *J. Electrochemical Soc.*, vol. 145, no. 4, p. 1318, 1998.

[62] H.-T. Chin et al., "Reaction-limited graphene CVD surpasses silicon production rate," *2D Mater.*, vol. 8, no. 3, Jul. 2021, Art. no. 035016.

[63] T. Goto, "High temperature passive oxidation mechanism of CVD SiC," *Mater. Sci. Forum*, vols. 522–523, pp. 27–36, Aug. 2006.

[64] T. Narushima, T. Goto, and T. Hirai, "High-temperature passive oxidation of chemically vapor deposited silicon carbide," *J. Amer. Ceram. Soc.*, vol. 72, no. 8, pp. 1386–1390, Aug. 1989.

[65] H. Nagasawa and K. Yagi, "3C-SiC single-crystal films grown on 6-Inch Si substrates," *Phys. Status Solidi (B)*, vol. 202, no. 1, pp. 335–358, Jul. 1997.

[66] C. A. Zorman, S. Rajgopal, X. A. Fu, R. Jezeski, J. Melzak, and M. Mehregany, "Deposition of polycrystalline 3C-SiC films on 100 mm diameter Si(100) wafers in a large-volume LPCVD furnace," *Electrochemical Solid-State Lett.*, vol. 5, no. 10, p. G99, 2002.

[67] H. Zheng, J. Su, Z. Fu, G. Li, and X. Li, "Heteroepitaxial growth and characterization of 3C-SiC films on on-axis Si (110) substrates by LPCVD," *Ceram. Int.*, vol. 34, no. 3, pp. 657–660, Apr. 2008.

[68] X.-A. Fu, J. L. Dunning, C. A. Zorman, and M. Mehregany, "Polycrystalline 3C-SiC thin films deposited by dual precursor LPCVD for MEMS applications," *Sens. Actuators A, Phys.*, vol. 119, no. 1, pp. 169–176, Mar. 2005.

[69] H. Kikuchi, R. K. Kalia, A. Nakano, P. Vashishta, P. S. Branicio, and F. Shimojo, "Brittle dynamic fracture of crystalline cubic silicon carbide (3C-SiC) via molecular dynamics simulation," *J. Appl. Phys.*, vol. 98, no. 10, Nov. 2005, Art. no. 103524.

[70] T. Nishiguchi, M. Nakamura, K. Nishio, T. Isshiki, and S. Nishino, "Heteroepitaxial growth of (111) 3C–SiC on well-lattice-matched (110) Si substrates by chemical vapor deposition," *Appl. Phys. Lett.*, vol. 84, no. 16, pp. 3082–3084, Apr. 2004.

[71] H. A. Calderon, A. Okonkwo, I. Estrada-Guel, V. G. Hadjiev, F. Alvarez-Ramírez, and F. C. Robles Hernández, "HRTEM low dose: The unfold of the morphed graphene, from amorphous carbon to morphed graphenes," *Adv. Struct. Chem. Imag.*, vol. 2, no. 1, p. 10, Dec. 2016.

[72] H. B. Rosenstock, "Dynamics of the graphite lattice," *J. Chem. Phys.*, vol. 21, no. 11, pp. 2064–2069, Nov. 1953.

[73] J. D. Bernal, "The structure of graphite," *Proc. Roy. Soc. London. Ser. A, Containing Papers Math. Phys. Character*, vol. 106, no. 740, pp. 749–773, 1924.

[74] A. J. Steckl, C. Yuan, J. P. Li, and M. J. Loboda, "Growth of crystalline 3C-SiC on Si at reduced temperatures by chemical vapor deposition from silacyclobutane," *Appl. Phys. Lett.*, vol. 63, no. 24, pp. 3347–3349, Dec. 1993.

[75] G.-S. Chung and K.-S. Kim, "Characteristics of poly-crystalline 3C-SiC thin films grown for micro/nano-electromechanical systems by using single-precursor hexamethyldisilane," *J. Korean Phys. Soc.*, vol. 51, no. 4, p. 1389, Oct. 2007.

[76] H. Zheng, Z. Fu, B. Lin, and X. Li, "Controlled-growth and characterization of 3C-SiC and 6H-SiC films on C-plane sapphire substrates by LPCVD," *J. Alloys Compounds*, vol. 426, nos. 1–2, pp. 290–294, Dec. 2006.

[77] S. Noh, X. Fu, L. Chen, and M. Mehregany, "A study of electrical properties and microstructure of nitrogen-doped poly-SiC films deposited by LPCVD," *Sens. Actuators A, Phys.*, vol. 136, no. 2, pp. 613–617, May 2007.

[78] X.-A. Fu, J. Trevino, M. Mehregany, and C. A. Zorman, "Doped polycrystalline 3C–SiC films with low stress for MEMS: Part I. Deposition conditions and film properties," *J. Micromech. Microeng.*, vol. 24, no. 3, Mar. 2014, Art. no. 035013.

[79] J. Zhang, R. T. Howe, and R. Maboudian, "Electrical characterization of n-type polycrystalline 3C-silicon carbide thin films deposited by 1,3-disilabutane," *J. Electrochemical Soc.*, vol. 153, no. 6, p. G548, 2006.

[80] G.-S. Chung and K.-H. Yoon, "Ohmic contacts to single-crystalline 3C-SiC films for extreme-environment MEMS applications," *Microelectron. J.*, vol. 39, no. 12, pp. 1408–1412, Dec. 2008.

[81] J. S. Chen, A. Bächli, M.-A. Nicolet, L. Baud, C. Jaussaud, and R. Madar, "Contact resistivity of Re, Pt and Ta films on n-type β-SiC: Preliminary results," *Mater. Sci. Eng., B*, vol. 29, nos. 1–3, pp. 185–189, Jan. 1995.

[82] G. Constantinidis, N. Kornilios, K. Zekentes, J. Stoemenos, and L. di. Cioccio, "High temperature ohmic contacts to 3C-SiC grown on Si substrates by chemical vapor deposition," *Mater. Sci. Eng., B*, vol. 46, nos. 1–3, pp. 176–179, Apr. 1997.

[83] L. L. Kazmerski, *Electrical Properties of Polycrystalline Semiconductor Thin Films*. New York, NY, USA: Academic, 1980.

[84] M. Zielinski, M. Portail, T. Chassagne, S. Juillaguet, and H. Peyre, "Nitrogen doping of 3C-SiC thin films grown by CVD in a resistively heated horizontal hot-wall reactor," *J. Cryst. Growth*, vol. 310, no. 13, pp. 3174–3182, Jun. 2008.